

Locally Sustainable Biodiesel Production from Waste Cooking Oil and Grease Using a Deep Eutectic Solvent: Characterization, Thermal Properties, and Blend Performance

Neelam Khan,* Sang H. Park, Lorraine Kadima, Carlove Bourdeau, Evelyn Calina, Charles Warren Edmunds, and David P. Pursell



Cite This: *ACS Omega* 2021, 6, 9204–9212



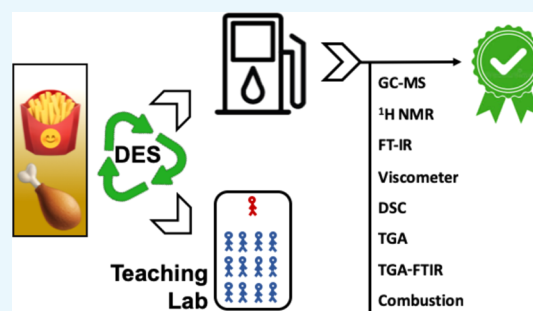
Read Online

ACCESS |

Metrics & More

Article Recommendations

ABSTRACT: As part of local sustainability efforts, biodiesel was synthesized via transesterification using a deep eutectic solvent (DES) without further washing from on-campus, dining facility waste cooking oil and grease. Before moving forward with repurposing used DES as a solvent in chemistry teaching labs, we determined the suitability of the biodiesel as an alternative fuel blended with diesel to power campus utility vehicles. Biodiesel components were characterized by gas chromatography–mass spectrometry (GC–MS), Fourier transform infrared spectroscopy (FTIR), nuclear magnetic resonance spectroscopy (^1H NMR), viscometer, differential scanning calorimetry (DSC), and evolved gas analysis during pyrolysis with a thermogravimetric analyzer coupled with FTIR (TGA–FTIR). The four major components of fatty acid methyl esters (FAMES) in the biodiesel were methyl oleate, methyl linoleate, methyl palmitate, and methyl stearate. Kinematic viscosity over typical temperature ranges was within optimal values recommended by the American Biodiesel Standard (ASTM D6751), with a 30:70 biodiesel/diesel blend experimental viscosity of 3.43 cSt at 40 °C and a calculated viscosity of 10.13 cSt at 0 °C. The pure biodiesel's cold-temperature onset of crystal formation is -10.1 °C versus -16.4 °C for a 30:70 biodiesel/diesel blend. Pyrolysis indicates good thermal stability, however, with an increased CO_2 evolution in the blended fuel at higher temperatures as compared to that in the pure biodiesel and the pure diesel. Combustion gas analysis indicates virtually complete combustion of the blended fuel to CO_2 and H_2O with only trace amounts of CO. Overall results indicate that the biodiesel synthesized using DES is a suitable fuel for campus utility vehicles in the local moderate temperature climate and affords increased local sustainability by using used DES repurposed in our chemistry teaching labs.



1. INTRODUCTION

Biofuels have achieved a measure of acceptance and are used across many industries, including the military. In fact, the U.S. Navy operated an entire fleet with an aircraft carrier, its aircraft, and support ships using biofuels; the fleet performed at the same level as when using petroleum-based fuels, although at a higher cost.¹ Biofuels are produced from a variety of sources to include vegetable oils, ethanol, algae, wood stock, and waste products from human activities. Biodiesel is a sustainable alternative to petroleum diesel fuel, especially when using feedstock from nonedible oils that do not compete with food production, which is particularly important in developing economies.² To increase production capacity from nonedible feedstocks, there has been much work recently on enzymatic conversion of sea-borne algae into biodiesel.³ Nevertheless, investigations continue in more traditional approaches using transesterification of triglycerides, from either pure oils or waste cooking oil and grease, into fatty acid methyl/ethyl esters.^{4–7} The generation of glycerol-based byproducts of

transesterification synthesis is problematic, as these byproducts often require additional resources and further processing to become useful materials rather than waste needing disposal, all of which increases costs and reduces sustainability aspects of biodiesel.⁸

One approach to minimize nonuseful byproducts of transesterification is by incorporating deep eutectic solvents (DESs) in the production process, such as choline chloride/glycerol in the presence of a base. The DES efficiently extracts excess glycerol from the biodiesel product, reducing production costs associated with isolating, washing, and drying

Received: January 30, 2021

Accepted: March 11, 2021

Published: March 25, 2021



the biodiesel product. In addition, the DES may be recycled for use multiple times in the production process.^{9–13} Many local communities, including college campuses such as ours, emphasize local sustainability practices. Biodiesel synthesis from waste cooking oil and grease using DES supports these practices as the biodiesel may be used as a locally sourced alternative to petroleum diesel to power campus operations, maintenance, and security utility vehicles.¹⁴ As an added benefit, after multiple uses in the biodiesel production process, the used DESs may be repurposed as green solvents in our undergraduate chemistry teaching laboratories for Diels–Alder, olefin cross-metathesis, ring-closing metathesis, and many other reactions, further reducing operating costs of our chemistry program while emphasizing local sustainability practices.^{9,15,16}

Our objective with this current investigation is to ensure that biodiesel produced from our local dining hall waste cooking oil and grease via base-catalyzed transesterification using a DES is suitable for use as a fuel and is of a character similar to our biodiesel produced without DES. To accomplish this, we will report on the composition of the biodiesel and biodiesel/diesel blends by gas chromatography–mass spectrometry (GC–MS) and nuclear magnetic resonance spectroscopy (¹H NMR) and their key properties of viscosity (viscometer), cold-temperature crystallization (differential scanning calorimetry (DSC)), pyrolysis, and evolved gases (thermogravimetric analysis–Fourier transform infrared spectroscopy (TGA-FTIR)) and finally a brief analysis of combustion exhaust gas (FTIR) while using the biodiesel/diesel blended fuel to power a diesel generator.

2. RESULTS AND DISCUSSION

2.1. GC–MS Analysis. The fatty acid methyl esters (FAMES) profile of the biodiesel generated from waste cooking oil and grease was determined by the GC–MS analysis method described in Section 4. The retention times of individual peaks of the gas chromatogram were verified against a FAME standard mixture, and individual FAMES were identified using the MS database (NIST library data). The combined waste cooking oil and grease was generated from pure canola oil and pure peanut oil used in the cooking process of the campus dining facility. C18 fatty acids are the major fatty acid constituents of the synthesized biodiesel with the identified FAMES being methyl oleate, methyl linoleate, methyl palmitate, and methyl stearate, and their analysis and identification are consistent with previous studies.^{14,17,18} The biodiesel synthesized using DES FAME composition is shown in Table 1, and GC chromatogram is shown in Figure 1.

2.2. NMR Analysis. The ¹H NMR results [δ /ppm] are as follows: $\delta = 0.88$, triplet, 3H, $-\text{CH}_3$; $\delta = 1.28$, singlet, 22H,

aliphatic CH_2 ; $\delta = 2.02$, multiplet, 2H, $-\text{CH}_2-\text{C}_{\text{sp}^2}\text{H}$; $\delta = 2.22$, triplet, 2H, $\text{O}=\text{C}-\text{CH}_2-$; $\delta = 2.80$, triplet, 1H, $-\text{HC}_{\text{sp}^2}-\text{CH}_2-\text{C}_{\text{sp}^2}\text{H}-$; $\delta = 3.55$, singlet, 3H, $\text{CH}_3-\text{O}-$; and $\delta = 5.31$, multiplet, 2H, $-\text{CH}=\text{CH}-$. These results are consistent with our ¹H NMR (Bruker, 600 MHz) results for a mixture of FAME molecules resulting from the transesterification of waste cooking oil and grease without using DES, as well as other biodiesel ¹H NMR results.^{7,14,19,20}

2.3. Temperature-Dependent Kinematic Viscosity.

Figure 2 shows the variation of experimental kinematic viscosities for B100, B30, and ultralow sulfur diesel (ULSD) with temperature. Kinematic viscosities for B100 and ULSD were 5.31 and 2.59 cSt at 40 °C, meeting the B100 viscosity range (1.9–6 cSt) at 40 °C from the American Biodiesel Standard (ASTM D6751).²¹ The kinematic viscosity of B30 at 40 °C was 3.43 cSt, which is comparable to our previous result of 3.1 cSt for biodiesel synthesis without DES.¹⁴ It increases with a decrease in temperature, which is important in cold weather environments as high viscosity impacts flow through the fuel system and particularly fuel injection and nebulization.

To further investigate the low-temperature viscosity of our biodiesel using the DES, we used the experimental data to develop a fitted equation that enables the calculation of viscosity in the temperature regime where DSC data indicates the onset of crystallization. The experimental values of viscosity were fitted according to eq 1, which is the modified Andrade-type regression equation to characterize the temperature dependence of kinematic viscosity^{22–24}

$$\ln(\eta) = A + \frac{B}{T} + \frac{C}{T^2} \quad (1)$$

where η is the kinematic viscosity in cSt, A , B , and C are constants for each specific fluid, and T is the temperature in K. Equation 1 can be considered as a second-order polynomial equation in $1/T$. Figure 3 shows the graph of $\log_e(\eta)$ and inverse temperature (T).

The values of constants A , B , and C are derived using the polynomial curve fitting of the graph. Table 2 reports the values of constants for ULSD, B100, and B30. R^2 values indicate that our experimental data is a good fit with the regression equation (eq 1).

Using eq 1 and correlation constants, we calculated low-temperature kinematic viscosity values in a temperature range -20 to 10 °C, as shown in Table 3. Previous researchers have experimentally determined low-temperature viscosity for low sulfur petroleum diesel, pure FAMES (to include the individual components of our biodiesel), and biodiesel/diesel blends.²⁵

The two major components of our biodiesel are methyl oleate and methyl linoleate. For a 50:50 blend of methyl oleate/methyl linoleate, these researchers obtained a kinematic viscosity of 19.50 cSt at -10 °C and 13.05 cSt at 0 °C, which are comparable to our calculated values at these temperatures. For a 30:70 blend of methyl linoleate/commercial low sulfur diesel, they obtained a kinematic viscosity of 9.51 cSt at 0 °C, comparable to our calculated value of 10.13 cSt at 0 °C for B30. Our calculated low-temperature kinematic viscosity is therefore reasonable, especially for 0 °C and higher and, in this case, close to the accepted range of kinematic viscosity for biodiesel at 40 °C. From this, we anticipate that our biodiesel production using DES produces a B30 blended fuel with viscosity properties that enable the operation of campus vehicles virtually year-round in the moderate Georgia climate.

Table 1. FAME Composition of Biodiesel Synthesized from Waste Cooking Oil and Grease Using DES

retention time (min)	FAMES	structure	molecular weight	weight (%)
12.60	methyl palmitate	C16:0	270	13.7
14.08	methyl linoleate	C18:2 (9Z, 12Z)	294	24.3
14.13	methyl oleate	C18:1 (Cis-9)	296	53.7
14.36	methyl stearate	C18:0	298	8.3



Figure 1. GC chromatogram of fatty acid methyl esters of biodiesel synthesized from waste cooking oil and grease (DB-5 ms column).

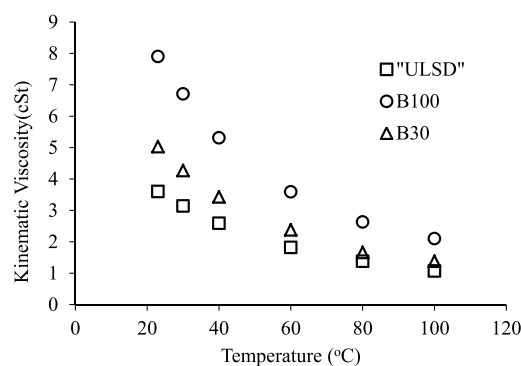


Figure 2. Variation of experimental kinematic viscosity with temperature for ULSD, B100, and B30.

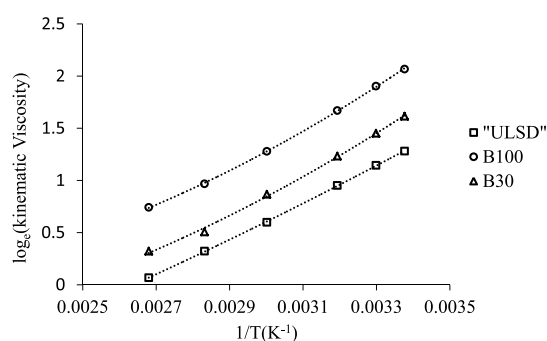


Figure 3. Variation of \log_e of experimental kinematic viscosity with inverse temperature for ULSD, B100, and B30.

Table 2. Viscosity Correlation Constants for ULSD, B100, and B30

fuel type	A	B	C	R ²
ULSD	-2.8799	587.19	191 412	0.9999
B30	0.2209	-1446.9	551 532	0.9982
B100	1.2555	-1872.7	626 512	0.9998

2.4. DSC Analysis. The B100 DSC cooling curve in Figure 4 shows two events. The first event begins with a peak onset at -10.1 °C and includes a second peak with an onset at -18.7 °C. These two peaks are part of the broad initial first event in the B100 cooling curve, may be viewed as the onset of liquid–liquid crystallization in sequence of the samples' saturated fatty acids methyl stearate (C18:0; 8.2%) with a ΔH of -6.62 J/g ($-\Delta H$ exothermic) followed by methyl palmitate (C16:0; 13.7%) with a ΔH of -19.9 J/g. The second event in the B100 curve is an intense and sharp peak beginning at -57.6 °C and

represents freezing of the unsaturated components methyl linoleate (C18:2-9Z,12Z; 24.3%) and methyl oleate (C18:1-9Z; 53.7%) with a ΔH of -54.8 J/g. The ULSD cooling curve shows one event with an onset of -19.2 °C for a sharp initial peak followed by a broad tail and represents the onset of crystal formation with a ΔH of -6.66 J/g. The B30 cooling curve shows one event in a broad feature with an onset of -16.4 °C and represents the onset of crystal formation in the blended fuel with a ΔH of -13.2 J/g. The DSC results for B100 produced from waste cooking oil and grease are consistent with other works. B100 has a total degree of unsaturation (DU) of 102.5, calculated following the procedure of other researchers.^{6,26–28} The B100 sample included two distinct features, including a broad peak for the first event with an onset of -10.1 °C and the second event exhibited a sharp feature with an onset at -57.6 °C. These are consistent with other findings, indicating a higher-onset temperature for saturated components and a lower-onset temperature for unsaturated components.^{29,30} The B100 onset of -10.1 °C is in general agreement with the DU trends found for methyl tallowate (DU 73.6, onset 7.0 °C), soybean oil methyl ester (DU 84.5, onset 2.20 °C), hemp methyl ester (DU 128.5, onset -5.27 °C), methyl soyate (DU 143.8, onset -6.5 °C), and *Aleurites moluccanus* methyl ester (DU 180.4, onset -9.96 °C).^{28,30,31}

The addition of our biodiesel to ULSD to produce the B30 blend decreases the crystallization onset temperature by 6.3 °C compared to that of pure biodiesel, from -10.1 °C for B100 to -16.4 °C for B30, and is consistent with similar trends for biodiesel/diesel blends versus diesel found by other researchers.^{6,28,32} These observations support the idea that crystallization of these fuels depends on the spatial arrangement, length, and degree of saturation of the fatty acid chains, which inhibit the molecular packing leading to lower crystallization onset temperatures, and that adding diesel to biodiesel results in a crystallization onset temperature lower than pure biodiesel but higher than pure diesel.^{5,26,28,29,33,34} The DSC cooling curve results shown in Figure 4 are summarized in Table 4.

2.5. TGA-FTIR Analysis. The TGA weight loss and derivative weight loss curves shown in Figure 5 indicate a continuous weight loss event for ULSD, B100, and B30 with the samples containing biodiesel showing stages in the single weight loss event. The ULSD curve shows one continuous weight loss event with an onset of 119 °C, maximum weight loss at 211 °C, and encompasses 98.6% of the weight. The B100 curve shows one continuous weight loss event with three stages, a major stage followed by two smaller stages occurring at higher temperatures. The B100 major weight loss stage has

Table 3. Comparison of Experimental and Calculated Kinematic Viscosities

temp (K)	temp (°C)	experimental kinematic viscosity (cSt)			calculated kinematic viscosity (cSt) Andrade's equation			absolute-difference (exp – calc)		
		ULSD	B100	B30	ULSD	B100	B30	ULSD	B100	B30
253.15	−20				11.3	37.9	22.5			
263.15	−10				8.29	24.20	14.7			
273.15	0				6.27	16.4	10.13			
283.15	10				4.86	11.7	7.32			
296.15	23	3.60	7.9	5.03	3.62	7.96	5.07	0.02	0.06	0.04
303.15	30	3.14	6.71	4.27	3.13	6.65	4.26	0.01	0.06	0.01
313.15	40	2.59	5.31	3.43	2.58	5.28	3.40	0.01	0.03	0.03
333.15	60	1.82	3.59	2.38	1.84	3.59	2.33	0.02	0.00	0.05
353.15	80	1.38	2.63	1.66	1.37	2.65	1.72	0.01	0.02	0.06
373.15	100	1.07	2.1	1.38	1.08	2.09	1.36	0.01	0.01	0.02

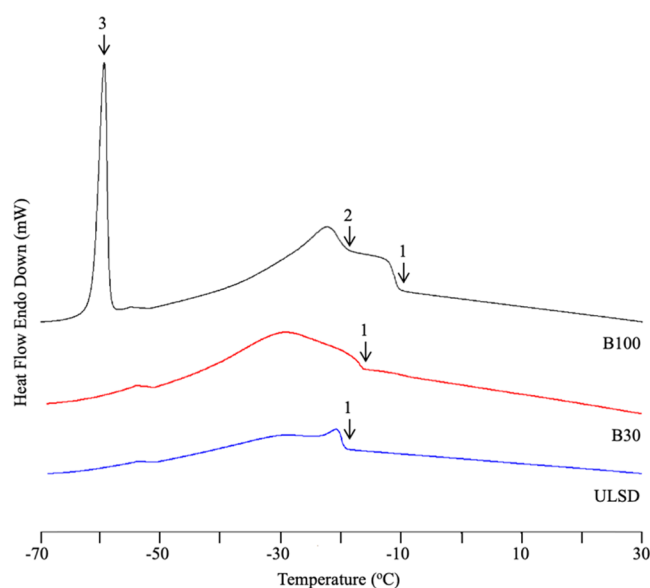


Figure 4. DSC cooling curves with peak onsets 1, 2, and 3 indicated.

an onset of 230 °C, maximum weight loss at 264 °C, and encompasses 86.6% of the weight. The onset of the B100 second weight loss stage is 296 °C, maximum weight loss at 341 °C, and encompasses 10.4% of the weight. The third stage for B100 has an onset of 391 °C, maximum weight loss at 437 °C, and encompasses 2.9% of the weight. The continuous B100 weight loss event with three stages encompasses 99.9% of the total weight.

The B30 curve has a single weight loss event with two stages. The B30 first stage onset is 154 °C with a maximum weight loss at 248 °C and encompasses 93.5% of the weight, while the second stage onset is 337 °C with a max weight loss at 387 °C and encompasses 5.9% of the weight. The continuous B30 weight loss event with two stages encompasses 99.4% of the weight. This second stage of the B30 weight loss is noteworthy as it corresponds to increased CO₂ evolution and will be

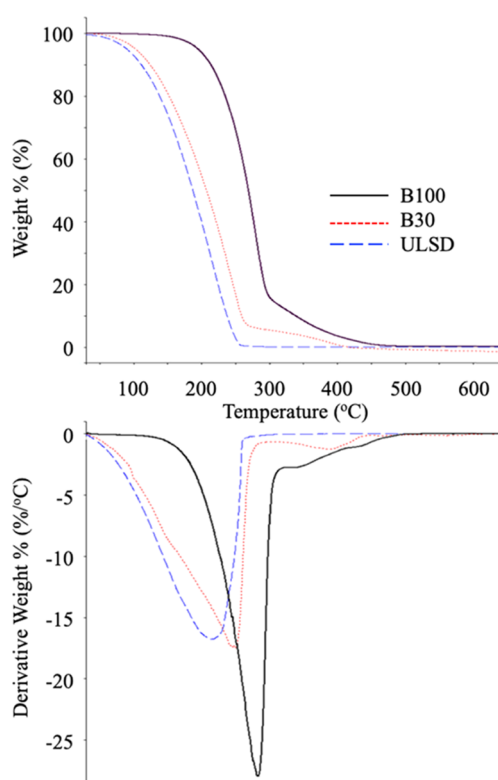


Figure 5. TGA weight loss and derivative weight loss curves.

discussed in more detail in the TGA-FTIR evolved gas analysis. The TGA weight loss results are summarized in Table 5.

Researchers have found similar weight loss curves for diesel, biodiesel/diesel blends, and biodiesel. Diesel typically has the lowest onset temperature (50–120 °C depending on the source and composition of the diesel), followed by biodiesel/diesel blends, which have a higher-onset temperature than diesel. Biodiesel typically has a higher-onset temperature than the blends, and depending on the biodiesel source and DUs,

Table 4. DSC Cooling Curve Data Summary

	event 1			event 2					
	onset T (°C)	peak T (°C)	ΔH (J/g)	onset T (°C)	peak T (°C)	ΔH (J/g)	onset T (°C)	peak T (°C)	ΔH (J/g)
ULSD	−19.2	−20.7	−6.66						
B30	−16.4	−29.1	−13.2						
B100	−10.1	−12.5	−6.62	−18.7	−22.0	−19.9	−57.6	−58.5	−54.8

Table 5. TGA Weight Loss Curve Data Summary

	stage 1			stage 2			stage 3		
	onset T ($^{\circ}\text{C}$)	max wt loss T ($^{\circ}\text{C}$)	wt loss (%)	onset T ($^{\circ}\text{C}$)	max wt loss T ($^{\circ}\text{C}$)	wt loss (%)	onset T ($^{\circ}\text{C}$)	max wt loss T ($^{\circ}\text{C}$)	wt loss (%)
ULSD	119	211	98.6						
B30	154	248	93.5	337	387	5.9			
B100	230	264	86.6	296	341	10.4	391	437	2.9

the onset ranges from 150 to 230 $^{\circ}\text{C}$.^{27,35–40} These researchers noted only one continuous weight loss event for diesel, biodiesel/diesel blends, and biodiesel. However, researchers examining waste cooking oil and grease biodiesel with a DU of 110.58 found a single continuous weight loss event, while their derivative weight loss curve exhibited four stages, similar to the three stages we describe.²⁶ For their biodiesel, they found the first stage onset of 191.9 $^{\circ}\text{C}$ with a max weight loss at 270 $^{\circ}\text{C}$ and although not reported but displayed in their derivative weight loss curves, their second stage has a max weight loss at 380 $^{\circ}\text{C}$, the third stage has a max weight loss at 430 $^{\circ}\text{C}$, and the fourth stage has a max weight loss at 550 $^{\circ}\text{C}$. These observations are consistent with the findings for our B100 from waste cooking oil and grease with a DU of 102.5, the first stage onset at 230 $^{\circ}\text{C}$, the second stage max weight loss at 341 $^{\circ}\text{C}$, and the third stage max weight loss at 437 $^{\circ}\text{C}$. In total, these results are consistent with the notion that the larger and more complex the molecules in the fuel—including chain length, degree of unsaturation, E/Z confirmation, and extent of intermolecular attractive forces—the higher the onset temperature and, in general, reflect the colligative property of the boiling point elevation of solute/solvent mixtures.

The FTIR and TGA-FTIR spectra in Figure 6 provide information about the liquid samples of ULSD, B30, and B100

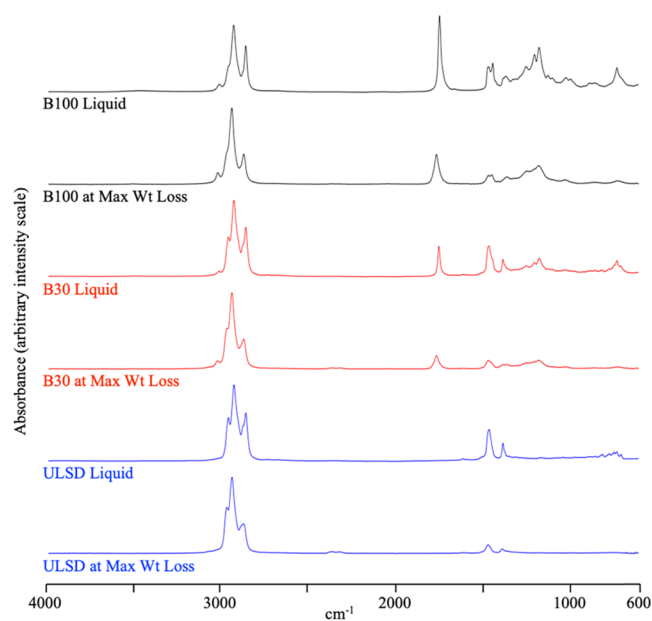


Figure 6. FTIR spectra of liquid samples compared to those of gas phase at maximum TGA weight loss events.

and the evolved gasses during weight loss events upon heating. The ULSD liquid shows the typical C–H alkane stretching modes at 2950, 2922, and 2850 cm^{-1} ; C–H alkane bending, scissor, and wagging modes at 1458 and 1378 cm^{-1} ; it lacks the C–H alkene stretching modes at just greater than 3000 cm^{-1} ,

indicating that the ULSD is composed of fully saturated hydrocarbons; it lacks the strong and broad feature of O–H stretching modes at 3400 cm^{-1} , indicating that the ULSD is free of water; and important for contrast with the B30 and B100 samples, it lacks the C=O ester stretching mode at 1745 cm^{-1} . The B100 liquid shows the C–H alkene mode at 3017 cm^{-1} , indicating the unsaturation of components in the mixture in agreement with the GC–MS and ^1H NMR results; the C–H alkane stretching modes at 2950, 2922, and 2850 cm^{-1} ; C–H alkane bending, scissor, and wagging modes at 1458 and 1378 cm^{-1} ; it has an intense C=O methyl ester mode at 1745 cm^{-1} ; the O–CH₃ asymmetric deformation mode of the methyl ester at 1435 cm^{-1} ; and quite significantly, it lacks the strong and broad feature of the O–H stretching mode at 3400 cm^{-1} , indicating that the B100 is free of water and glycerol, even though our production process with DES included only the separatory funnel segregation of components and no washing and drying of the biodiesel product. As expected, the B30 liquid spectra possess modes of both the ULSD and the B100 and it is free of water and glycerol as well. The FTIR spectra of Figure 6 for the first stage max weight loss events of ULSD (211 $^{\circ}\text{C}$), B30 (248 $^{\circ}\text{C}$), and B100 (264 $^{\circ}\text{C}$) are essentially identical to those for the corresponding liquid ULSD, B30, and B100, indicating volatilization of the sample components during the pyrolysis. For all three samples, the majority of the weight is lost in this first stage as discussed in the TGA results and is summarized in Table 5.

In addition, the first stage max weight loss of the ULSD (211 $^{\circ}\text{C}$) exhibits a small quantity of CO₂, indicated by the CO₂ asymmetric stretching mode at 2343 cm^{-1} and the CO₂ bending mode at 668 cm^{-1} . In contrast to the ULSD, the first stage max weight loss of the B30 (248 $^{\circ}\text{C}$) and B100 (264 $^{\circ}\text{C}$) displays only the slightest hint of these CO₂ vibrational modes. Figure 7 shows 3-D (intensity–wavenumber–temperature) plots and demonstrates that as the temperature is increased after the first stage weight loss event for the ULSD, the intensity of C–H alkane bending, scissor, and wagging modes at 1458 and 1378 cm^{-1} is significantly reduced and in proportion to the reduction of the C–H alkane stretching modes at 2950, 2922, and 2850 cm^{-1} .

The intensity of the ULSD CO₂ modes increases slightly to a relatively constant but small amount up to a maximum temperature of 650 $^{\circ}\text{C}$. As the temperature is increased for the B100, stage 2 and stage 3 of the continuous weight loss events occur with the continued presence of the ester mode at 1745 cm^{-1} , indicating that carbonyl compounds, and perhaps the full FAMES, continue to volatilize even up to a maximum temperature of 650 $^{\circ}\text{C}$. For B100, the intensity of the CO₂ vibrational modes remains constant and very low throughout the entire heating range, indicating very little production of CO₂ during pyrolysis. From these differences in the ULSD and B100 curves, one may conclude that the ULSD produces more CO₂ than the B100 as the pyrolysis continues to higher temperatures. These findings are similar to those of other researchers.^{26–28,30–35,41–44}

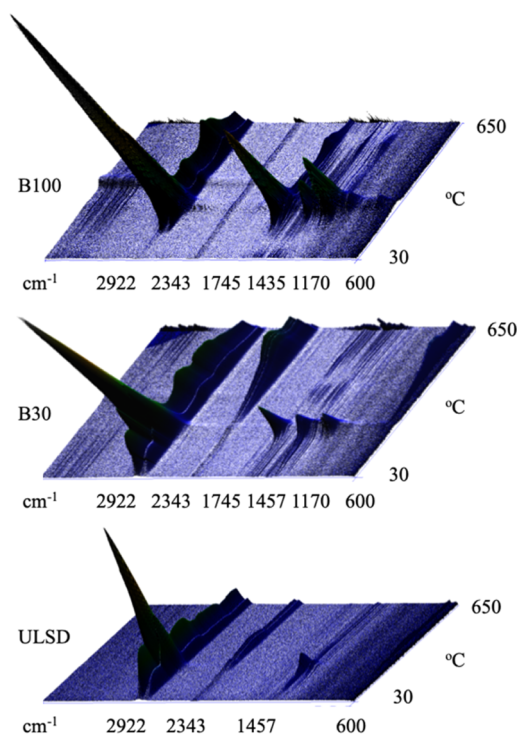


Figure 7. TGA-FTIR spectra of liquid samples and sample gas evolved over the heating range of 30–650 °C.

The spectra in Figure 7 for B30 throughout the temperature range present some interesting contrasts to those of the ULSD and B100. One would expect the B30 to demonstrate characteristics of both the ULSD and B100 pyrolysis spectra. Like the B100 spectrum, the B30 spectrum does indicate that most of the ester is lost in the initial stage of weight loss, but a very small amount of the ester is lost in the higher-temperature second stage as well, as indicated by the very low intensity ester C=O stretching mode at 1745 cm^{-1} at higher temperatures. Like the ULSD spectrum, the B30 spectrum also indicates that most of the diesel components are lost in the initial stage of weight loss, indicated by the sharp reduction in the C–H stretching modes and C–H bending, scissor, and wagging modes with only a slight intensity of these modes through the maximum heating temperature of 650 °C. However, unlike the ULSD and B100 spectra, the B30 spectrum has a significant increase in CO_2 evolution beginning at the stage 2 onset temperature of 337 °C, as indicated by the large increase in intensity of the 2343 and 668 cm^{-1} vibrational modes of CO_2 . This large increase in CO_2 evolution for B30, in comparison to that for ULSD and B100, continues from the stage 2 onset at 337 °C through heating all the way to 650 °C.

To further investigate this difference in CO_2 evolution for the B30 compared to that for B100, we examined the integrated area of the intensity of the ester C=O stretching mode at 1745 cm^{-1} and the CO_2 asymmetric stretching mode at 2342 cm^{-1} for B30 and B100 over the entire pyrolysis heating range from 30 to 650 °C. While the integrated area of the intensity of these modes is not a direct indication of the amount or concentration in the samples, comparison of these intensities does provide an indication of the relative differences in amounts. Based on the 30% biodiesel composition of the B30, one would expect the integrated area of the ester mode throughout the temperature range from 30 to 650 °C in the B100 to be approximately 3.3 times greater than the integrated

area of the ester mode throughout the temperature range in the B30. Our integrated area ratio result was 3.7, slightly larger than expected and indicating that perhaps some of the C=O in the ester moiety in B30 was evolving in some manner other than the direct volatilization of the FAME of the biodiesel. Similar analysis for the integrated intensity of the CO_2 mode over the entire heating range from 30 to 650 °C indicates that the B30 produces 8.2 times more CO_2 than the B100, as shown qualitatively in Figure 7. The ester C=O stretching mode and the CO_2 antisymmetric stretching mode we are comparing and contrasting are both intense features in the IR spectrum because of their large transition dipole moments, but one must be cautious to directly compare the two modes to determine absolute quantities or amounts of components. What is apparent is that the B30 ester C=O stretching mode is perhaps slightly less than expected, while the B30 CO_2 asymmetric stretching mode is substantially larger than expected in comparison to the B100. While these results require further investigation, one might perhaps conclude that in the B30 there is a chemical rearrangement or reaction between the diesel and FAME components that results in some of the ester moiety of the FAME evolving as CO_2 rather than as the carbonyl compound. As noted, this observation requires further investigation before drawing fully substantiated conclusions.

2.6. FTIR of Combustion Exhaust Gas Analysis. The FTIR combustion exhaust gas spectrum in Figure 8 shows

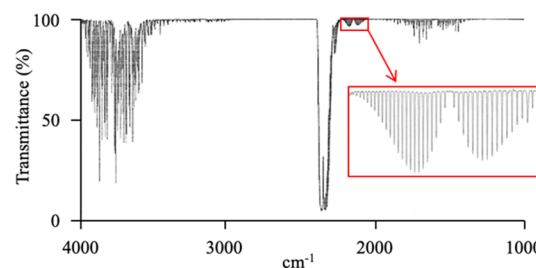


Figure 8. FTIR of diesel generator combustion exhaust gas fueled with B30. The inset shows the rotation–vibration band of CO.

signatures of three distinct gasses, CO_2 , H_2O , and CO.^{45–49} At the center of the spectrum is the sharp, intense feature of the CO_2 asymmetric stretch at 2348 cm^{-1} from combustion of the B30 in the generator. Just to the right of this CO_2 stretch is the low-intensity asymmetric stretch feature for $^{13}\text{CO}_2$ centered at 2284 cm^{-1} .

The other major features in the spectrum correspond to water, the combustion gas partner of CO_2 , with the H_2O asymmetric stretch at 3754 cm^{-1} , the symmetric stretch at 3655 cm^{-1} , and the broad bending–rotation band at 1594 cm^{-1} . In addition to CO_2 and H_2O , the spectrum also shows a low-intensity CO rotation–vibration band at 2143 cm^{-1} with the inset showing the distinct rotation–vibration signature of heteronuclear diatomic CO.³ There is no ester C=O stretching mode at 1743 cm^{-1} and only very slightest intensity of C–H alkane and alkene stretching modes from 2800 to 3200 cm^{-1} and CH_4 modes at 3030 cm^{-1} , indicating virtually complete combustion of the B30 in the generator to CO_2 and H_2O with insignificant amounts of other combustion products. These results are consistent with our combustion exhaust gas analysis using fuel synthesized from waste cooking oil and grease without using DES.¹⁴

3. CONCLUSIONS

Synthesis of biodiesel from waste cooking oil and grease using DES efficiently produces a locally sourced, sustainable fuel. The biodiesel requires no washing during production, offers multiple use recycling of the DES in repeated synthesis, and provides subsequent repurposing of the DES as a solvent for use in teaching laboratories. The GC–MS and ^1H NMR results indicate that the biodiesel synthesized using DES is a blend of saturated and unsaturated FAMES and in both, the pure biodiesel form and as a biodiesel/diesel blended fuel meet viscosity standards under normal climate temperatures. As cold-temperature operations are a practical concern, crystallization onset temperature determined via DSC is $-10.1\text{ }^\circ\text{C}$ for B100 and $-16.4\text{ }^\circ\text{C}$ for B30 as compared to that of $-19.2\text{ }^\circ\text{C}$ for ULSD, sufficient for year-round operations in Georgia and other similar climates. Likewise, the calculated cold-temperature viscosity for B30 at $0\text{ }^\circ\text{C}$ is 10.13 cSt, sufficient for cold-temperature flow through the vehicle fuel lines and injection system. TGA-FTIR pyrolysis experiments up to $650\text{ }^\circ\text{C}$ demonstrate good thermal stability for B100. The evolved gas analysis presents the interesting phenomenon for B30, during stage 2 of the weight loss, of perhaps chemical rearrangement or reaction between the diesel and the biodiesel FAME components to produce a larger than expected amount of CO_2 compared to pure B100 and pure diesel. The gas-phase FTIR of combustion exhaust while using the B30 fuel to power a diesel generator indicates nearly complete combustion to CO_2 and H_2O with only a very small quantity of CO and virtually no other combustion products. As a result, we conclude that the biodiesel synthesized from dining operations, waste cooking oil and grease using DES, is suitable for use as a blended fuel to power campus utility vehicles year-round in the local climate and contributes to our goal of local sustainability.

4. EXPERIMENTAL SECTION

4.1. Materials. Waste cooking oil and grease from the local on-campus fast food restaurants were the feedstock for the synthesized biodiesel using a DES. Methanol (certified ACS, Fisher Chemical), sodium hydroxide (certified ACS, Fisher Chemical), glycerol (certified ACS, Fisher Chemical), choline chloride (>98%, Alfa Aesar), a standard mixture of 37 FAMES (Restek Corporation), and dichloromethane (high-performance liquid chromatography (HPLC) grade, Acros) were purchased from Fisher Scientific (Somerville, NJ). The ultralow sulfur diesel (ULSD) fuel was obtained from a local commercial gasoline station.

4.2. Biodiesel Synthesis. Synthesis followed the general procedures of similar work.^{4,10,50,51} The DES was prepared with a 2:1 mole ratio of choline chloride/glycerol (34.2:25.8 g), stirred until well mixed. The DES was activated with NaOH (6 g of NaOH, which is 1% of the mass of waste oil and grease used, and the NaOH is crushed, ground, and dried in a $100\text{ }^\circ\text{C}$ oven for 12 h and cooled to room temperature prior to use), stirred until well mixed. The waste cooking oil and grease were vacuum-filtered (Fisherbrand filter paper, P4 grade) to remove nonfluid materials. After filtering, 600 g of waste cooking oil and grease was mixed with 120 g of methanol in a 1 L round-bottom flask, stirred under a condensing column, and heated to $65\text{ }^\circ\text{C}$. The activated DES (66 g) was added to the preheated waste cooking oil and grease/methanol mixture, stirred, and heated to $65\text{ }^\circ\text{C}$ under a condensing column for 3 h. The reaction mixture was transferred to a separatory funnel

and allowed to gradually cool to an ambient temperature ($22\text{ }^\circ\text{C}$) over 12 h while the reaction components were partitioned in the separatory funnel. Biodiesel (clear and slightly yellow color liquid, 466 g) was separated for analysis without any additional washing. Samples analyzed were a 100% ultralow sulfur diesel (sample name ULSD), a 100% biodiesel synthesized from waste cooking oil and grease using DES (sample name B100), and a 30:70 volume ratio mixture of the biodiesel synthesized from waste cooking oil and grease using DES and ULSD (sample name B30).

4.3. Gas Chromatography–Mass Spectrometry (GC–MS). The biodiesel samples were analyzed using a Shimadzu QP2010S Gas Chromatography–Mass Spectrometer (GC–MS) with a DB-5 ms column (30 m, 0.25 mm i.d., 0.25 μm film thickness) in scan mode to determine the fatty acid methyl ester (FAME) composition. The carrier gas was helium with a constant pressure of 52.0 kPa. The sample of 1.0 μL in methylene chloride was injected using split mode with a split ratio of 1:5 at an injection temperature of $250\text{ }^\circ\text{C}$. The GC oven temperatures were held at $50\text{ }^\circ\text{C}$ for 1 min and increased at $20\text{ }^\circ\text{C}/\text{min}$ to $200\text{ }^\circ\text{C}$ and $10\text{ }^\circ\text{C}/\text{min}$ to $250\text{ }^\circ\text{C}$ with finally holding for 10 min. The GC–MS interface was maintained at $250\text{ }^\circ\text{C}$, and the MS ion source temperature was $230\text{ }^\circ\text{C}$.

4.4. Nuclear Magnetic Resonance Spectroscopy (NMR). ^1H NMR scans were conducted using an Anasazi instruments Eft-90 (90 MHz) spectrometer interfaced to Anasazi aii 5.170.213 and NMR Utility Transform Software. Chemical shifts were referenced to an internal standard, tetramethylsilane (TMS), using CDCl_3 solvent.

4.5. Temperature-Dependent Kinematic Viscosity. Kinematic viscosity was measured according to the standard ASTM-D445 method. A Cannon-Ubbelohde viscometer along with a Poly-Science viscosity bath was used to collect the efflux time (time for biodiesel to flow a certain distance in the viscometer under gravity) for B100, B30, and ULSD at temperatures varying from room temperature to $100\text{ }^\circ\text{C}$. Kinematic viscosity was calculated by multiplying the efflux time with the viscometer calibration constant.

4.6. Differential Scanning Calorimeter (DSC). B100, B30, and ULSD were examined using DSC. Samples of 16.0 μg were sealed in aluminum pans, placed in the nitrogen-purged furnace with an adjacent reference sealed aluminum pan, cooled to $-70\text{ }^\circ\text{C}$, heated to $50\text{ }^\circ\text{C}$ at a rate of $10\text{ }^\circ\text{C}/\text{min}$, and then cooled to $-70\text{ }^\circ\text{C}$ at a rate of $10\text{ }^\circ\text{C}/\text{min}$ using a PerkinElmer DSC6000. PerkinElmer Pyris software controlled the DSC.

4.7. Thermogravimetric Analysis Coupled with Infrared Spectroscopy (TGA-FTIR). B100, B30, and ULSD were examined using TGA-FTIR for evolved gas analysis. Samples of 25.0 μL in alumina crucibles were used with a PerkinElmer TGA 8000. A TL8000 transfer line maintained at $270\text{ }^\circ\text{C}$ coupled the TGA to a PerkinElmer Frontier FTIR with a 10 cm gas cell. Nitrogen was the purge gas through the TGA with a balance purge flow rate of 70 mL/min and a sample purge rate of 50 mL/min. The TGA temperature was increased at $10\text{ }^\circ\text{C}/\text{min}$ from 30 to $650\text{ }^\circ\text{C}$. Infrared spectra were collected at 55 scans/min over the range of $4000\text{--}600\text{ cm}^{-1}$ at a 4 cm^{-1} resolution. The TGA was controlled using PerkinElmer Pyris software, and PerkinElmer TimeBase controlled the IR.

4.8. Combustion Gas Fourier Transform Infrared Spectroscopy (FTIR). ULSD was used to power a Generac XD 5 kW diesel generator to operating temperatures, the fuel was then changed from ULSD to B30, and the combustion

exhaust gas was captured. A Schlenk line connected to a 10 cm gas cell with CaF₂ windows at 23 °C was evacuated to 0.5 Torr, and the combustion exhaust gas was then loaded into the line and gas cell to a pressure of 760 Torr at 23 °C. The exhaust gas was analyzed with a PerkinElmer Spectrum One spectrophotometer from 4000 to 1000 cm⁻¹ at a 0.5 cm⁻¹ resolution using signal averaging over 64 scans.

AUTHOR INFORMATION

Corresponding Author

Neelam Khan – School of Science and Technology, Georgia Gwinnett College, Lawrenceville, Georgia 30043, United States; orcid.org/0000-0002-8477-813X; Email: nkhan3@ggc.edu

Authors

Sang H. Park – School of Science and Technology, Georgia Gwinnett College, Lawrenceville, Georgia 30043, United States; orcid.org/0000-0001-6953-0681

Lorraine Kadima – School of Science and Technology, Georgia Gwinnett College, Lawrenceville, Georgia 30043, United States; orcid.org/0000-0001-6345-0779

Carlove Bourdeau – School of Science and Technology, Georgia Gwinnett College, Lawrenceville, Georgia 30043, United States; orcid.org/0000-0003-3423-561X

Evelyn Calina – School of Science and Technology, Georgia Gwinnett College, Lawrenceville, Georgia 30043, United States; orcid.org/0000-0001-7668-1330

Charles Warren Edmunds – PerkinElmer, John's Creek, Georgia 30097, United States; orcid.org/0000-0002-6129-2540

David P. Pursell – School of Science and Technology, Georgia Gwinnett College, Lawrenceville, Georgia 30043, United States; orcid.org/0000-0003-1922-5923

Complete contact information is available at:

<https://pubs.acs.org/10.1021/acsomega.1c00556>

Notes

The authors declare no competing financial interest.

REFERENCES

- (1) Chambers, A. M.; Yetiv, S. A. The Great Green Fleet. In *Naval War College Review*, 2011, Vol. 64, p 5.
- (2) Pinzi, S.; García, I.; López-Giménez, F. J.; Castro, M. D.; Dorado, G.; Dorado, M. The Ideal Vegetable Oil-based Biodiesel Composition: A Review of Social, Economical and Technical Implications. *Energy Fuels* **2009**, *23*, 2325–2341.
- (3) Hossain, S.; Razzak, S. A.; Alshater, A.; Moniruzzaman, M.; Hossain, M. M. Recent Advances in Enzymatic Conversion of Microalgal Lipids into Biodiesel. *Energy Fuels* **2020**, *34*, 6735–6750.
- (4) Cong, W.; Wang, Y.; Li, H.; Fang, Z.; Sun, J.; Liu, H.; Liu, J.; Tang, S.; Xu, L. Direct production of biodiesel from waste oils with a strong solid base from alkalinized industrial clay ash. *Appl. Energy* **2020**, *264*, No. 114735.
- (5) Uğuz, G.; Atabani, A. E.; Mohammed, M. N.; Shobana, S.; Uğuz, S.; Kumar, G.; Al-Muhtaseb, A. Fuel stability of biodiesel from waste cooking oil: A comparative evaluation with various antioxidants using FT-IR and DSC techniques. *Biocatal. Agric. Biotechnol.* **2019**, *21*, No. 101283.
- (6) Atabani, A. E.; Shobana, S.; Mohammed, M. N.; Uğuz, G.; Kumar, G.; Arvindnarayan, S.; Aslam, M.; Al-Muhtaseb, A. Integrated valorization of waste cooking oil and spent coffee grounds for biodiesel production: Blending with higher alcohols, FT-IR, TGA, DSC and NMR characterizations. *Fuel* **2019**, *244*, 419–430.

- (7) Carlson, J. S.; Monroe, E.; Dhaoui, R.; Zhu, J.; McEnally, C.; Shinde, S.; Pfefferle, L.; George, A.; Davis, R. Biodiesel Ethers: Fatty Acid Derived Alkyl Ether Fuels as Improved Bioblendstocks for Mixing-Controlled Compression Ignition Engines. *Energy Fuels* **2020**, *34*, 12646–12653.

- (8) Paiva, A.; Craveiro, R.; Aroso, I.; Martins, M.; Reis, R.; Duarte, A. Natural Deep Eutectic Solvents – Solvents for the 21st Century. *ACS Sustainable Chem. Eng.* **2014**, *2*, 1063–1071.

- (9) Smith, E. L.; Abbott, A. P.; Ryder, K. S. Deep eutectic solvents (DESs) and their applications. *Chem. Rev.* **2014**, *114*, 11060–11082.

- (10) Merza, F.; Fawzy, A.; AlNashef, I.; Al-Zuhair, S.; Taher, H. Effectiveness of using deep eutectic solvents as an alternative to conventional solvents in enzymatic biodiesel production from waste oils. *Energy Rep.* **2018**, *4*, 77–83.

- (11) Šalić, A.; Tusek, A.; Gojun, M.; Zelić, B. Biodiesel purification in microextractors: Choline chloride based deep eutectic solvents vs water. *Sep. Purif. Technol.* **2020**, *242*, No. 116783.

- (12) Gu, L.; Huang, W.; Tang, S.; Tian, S.; Zhang, X. A novel deep eutectic solvent for biodiesel preparation using a homogeneous base catalyst. *Chem. Eng. J.* **2015**, *259*, 647–652.

- (13) Liu, Y.; Hanzhao, Y.; Liu, J.; Dong, W.; Cao, Z.; Hu, X.; Zhou, Z. Acidic deep eutectic solvents with long carbon chains as catalysts and reaction media for biodiesel production. *Renewable Energy* **2020**, *162*, 1842–1853.

- (14) Park, S. H.; Khan, N.; Lee, S.; Zimmermann, K.; Derosa, M.; Hamilton, L.; Hudson, W.; Hyder, S. A.; Serratos, M.; Sheffield, E. C.; Veludhandi, A.; Pursell, D. Biodiesel Production from Locally Sourced Restaurant Waste Cooking Oil and Grease: Synthesis, Characterization, and Performance Evaluation. *ACS Omega* **2019**, *4*, 7775–7784.

- (15) Bumbaugh, R. E.; Ott, L. Preparing and Testing Novel Deep Eutectic Solvents from Biodiesel Co-Product Glycerol for Use as Green Solvents in Organic Chemistry Teaching Laboratories. *ACS Symp. Ser.* **2020**, *1351*, 113–130.

- (16) Florindo, C.; Oliveira, F. S.; Rebelo, L. P.; Fernandes, A.; Marrucho, I. Insights into the Synthesis and Properties of Deep Eutectic Solvents Based on Cholinium Chloride and Carboxylic Acids. *ACS Sustainable Chem. Eng.* **2014**, *2*, 2416–2425.

- (17) Kostik, V.; Memeti, S.; Bauer, B. Fatty acid composition of edible oils and fats. *J. Hyg. Eng. Des.* **2013**, *4*, 112–116.

- (18) Knothe, G.; Steidley, K. R. A comparison of used cooking oils: a very heterogeneous feedstock for biodiesel. *Bioresour. Technol.* **2009**, *100*, 5796–5801.

- (19) Zhao, H.; Zhang, C.; Crittle, T. D. Choline-based deep eutectic solvents for enzymatic preparation of biodiesel from soybean oil. *J. Mol. Catal. B* **2013**, *85–86*, 243–247.

- (20) Neiles, K. Y.; Bowers, G.; Chase, D. T.; VerMeulen, A.; Hovland, D. E.; Bresslour-Rashap, E.; Eller, L. R.; Koch, A. S. Teaching Collaborations and Scientific Practices through a Vertically Scaffolded Biodiesel Laboratory Experience. *J. Chem. Educ.* **2019**, *96*, 1988–1997.

- (21) Knothe, G.; Steidley, K. R. Kinematic viscosity of biodiesel fuel components and related compounds. Influence of compound structure and comparison to petrodiesel fuel components. *Fuel* **2005**, *84*, 1059–1065.

- (22) Tat, M. E.; Gerpen, J. V. The kinematic viscosity of biodiesel and its blends with diesel fuel. *J. Am. Oil Chem. Soc.* **1999**, *76*, 1511–1513.

- (23) Azian, M. N.; Kamal, A. A.; Panau, F.; Ten, W. K. Viscosity estimation of triacylglycerols and of some vegetable oils, based on their triacylglycerol composition. *J. Am. Oil Chem. Soc.* **2001**, *78*, 1001–1005.

- (24) Esteban, B.; Riba, J.; Baquero, G.; Rius, A.; Puig, R. Temperature dependence of density and viscosity of vegetable oils. *Biomass Bioenergy* **2012**, *42*, 164–171.

- (25) Knothe, G.; Steidley, K. R. Kinematic viscosity of biodiesel components (fatty acid alkyl esters) and related compounds at low temperatures. *Fuel* **2007**, *86*, 2560–2567.

- (26) Atabani, A. E.; Kulthoom, S. A. Spectral, thermoanalytical characterizations, properties, engine and emission performance of complementary biodiesel-diesel-pentanol/octanol blends. *Fuel* **2020**, *282*, No. 118849.
- (27) Atabani, A. E.; Al-Rubaye, O. K. Valorization of spent coffee grounds for biodiesel production: blending with higher alcohols, FT-IR, TGA, DSC, and NMR characterizations. *Biomass Convers. Biorefin.* **2020**, DOI: 10.1007/s13399-020-00866-z.
- (28) Bencheikh, K.; Atabani, A. E.; Shobana, S.; Mohammed, M. N.; Uğuz, G.; Arpa, O.; Kumar, G.; Ayanoglu, A.; Bokhari, A. Fuels properties, characterizations and engine and emission performance analyses of ternary waste cooking oil biodiesel–diesel–propanol blends. *Sustainable Energy Technol. Assess.* **2019**, *35*, 321–334.
- (29) Misutsu, M. Y.; Cavalheiro, L.; Ricci, T. G.; Viana, L. H.; Oliveira, S. C.; Júnior, A. M.; Oliveira, L. C. Thermoanalytical Methods in Verifying the Quality of Biodiesel. In *Biofuels—Status and Perspective*; IntechOpen, 2015; Chapter 12; pp 1164–1223.
- (30) Chen, W.; Wang, Y.; Ding, M.; Shi, S.; Yang, Z. Crystallization behaviors and rheological properties of biodiesel derived from methanol and ethanol. *Fuel* **2017**, *207*, 503–509.
- (31) Dunn, R. Thermal analysis of alternative diesel fuels from vegetable oils. *J. Am. Oil Chem. Soc.* **1999**, *76*, 109–115.
- (32) Dunn, R. Fuel Properties of Biodiesel/Ultra-Low Sulfur Diesel (ULSD) Blends. *J. Am. Oil Chem. Soc.* **2011**, *88*, 1977–1987.
- (33) Vijayan, S. K.; Victor, M. N.; Sudharsanam, A.; Chinnaraj, V. K.; Nagarajan, V. Winterization studies of different vegetable oil biodiesel. *Bioresour. Technol. Rep.* **2018**, *1*, 50–55.
- (34) García-Pérez, M.; Adams, T. T.; Goodrum, J.; Das, K. C.; Geller, D. P. DSC studies to evaluate the impact of bio-oil on cold flow properties and oxidation stability of bio-diesel. *Bioresour. Technol.* **2010**, *101*, 6219–6224.
- (35) Lazdoviča, K.; Liepiņa, L.; Kampars, V. Comparative wheat straw catalytic pyrolysis in the presence of zeolites, Pt/C, and Pd/C by using TGA-FTIR method. *Fuel Process. Technol.* **2015**, *138*, 645–653.
- (36) Li, H.; Niu, S.; Lu, C.; Wang, Y. Comprehensive Investigation of the Thermal Degradation Characteristics of Biodiesel and Its Feedstock Oil through TGA–FTIR. *Energy Fuels* **2015**, *29*, 5145–5153.
- (37) Dwivedi, G.; Sharma, M. Experimental investigation on thermal stability of Pongamia Biodiesel by thermogravimetric analysis. *Egypt. J. Pet.* **2016**, *25*, 33–38.
- (38) Chand, P.; Reddy, C. V.; Verkade, J.; Wang, T.; Grewell, D. Thermogravimetric Quantification of Biodiesel Produced via Alkali Catalyzed Transesterification of Soybean oil. *Energy Fuels* **2009**, *23*, 989–992.
- (39) Díaz-Ballote, L.; Gómez-Hernández, K.; Vega-Lizama, E.; Ruiz-Gómez, M. A.; Maldonado, L.; Hernández, E. Thermogravimetric approach for assessing the oxidation level of a biodiesel sample. *Quím. Nova* **2018**, *41*, 492–496.
- (40) Pragas, M. G.; Boey, P. L.; Shafida, A. H. Biodiesel from Adsorbed Waste Oil on Spent Bleaching Clay using CaO as a Heterogeneous Catalyst. *Eur. J. Sci. Res.* **2009**, *33*, 347–357.
- (41) Ong, H. C.; Chen, W.; Singh, Y.; Gan, Y.; Chen, C.; Show, P. L. A state-of-the-art review on thermochemical conversion of biomass for biofuel production: A TG-FTIR approach. *Energy Convers. Manage.* **2020**, *209*, No. 112634.
- (42) Jameel, A. G. A.; Han, Y.; Brignoli, O.; Telalović, S.; El-Baz, A.; Im, H.; Roberts, W. L.; Sarathy, S. M. Heavy fuel oil pyrolysis and combustion: Kinetics and evolved gases investigated by TGA-FTIR. *J. Anal. Appl. Pyrolysis* **2017**, *127*, 183–195.
- (43) Yang, H.; Yan, R.; Liang, D.; Chen, H.; Zheng, C. Pyrolysis of Palm Oil Wastes for Biofuel Production. *Asian J. Energy Environ.* **2006**, *7*, 315–323.
- (44) Li, H.; Feng-sheng, L.; Ma, X.; Cui, P.; Gao, Y.; Yu, M.; Guo, M. Effects of biodiesel blends on the kinetic and thermodynamic parameters of fossil diesel during thermal degradation. *Energy Convers. Manage.* **2019**, *198*, No. 111930.
- (45) Mahamuni, N. N.; Adewuyi, Y. G. Fourier Transform Infrared Spectroscopy (FTIR) Method To Monitor Soy Biodiesel and Soybean Oil in Transesterification Reactions, Petrodiesel–Biodiesel Blends, and Blend Adulteration with Soy Oil. *Energy Fuels* **2009**, *23*, 3773–3782.
- (46) Oliveira, J. S.; Montalvão, R.; Daher, L.; Suárez, P.; Rubim, J. C. Determination of methyl ester contents in biodiesel blends by FTIR-ATR and FTNIR spectroscopies. *Talanta* **2006**, *69*, 1278–1284.
- (47) Rank, D.; Pierre, A.; Wiggins, T. Rotational and vibration constants of CO. *J. Mol. Spectrosc.* **1965**, *18*, 418–427.
- (48) Mina-Camilde, N.; Manzanares, I.; Caballero, J. Molecular Constants of Carbon Monoxide at $v = 0, 1, 2$, and 3: A Vibrational Spectroscopy Experiment in Physical Chemistry. *J. Chem. Educ.* **1996**, *73*, 804–807.
- (49) Boyd, D.; Thompson, H. W.; Williams, R. Vibration-rotation bands of methane. *Proc. R. Soc. London, Ser. A* **1952**, *213*, 42–54.
- (50) Tremblay, A.; Cao, P.; Dubé, M. Biodiesel Production Using Ultralow Catalyst Concentrations. *Energy Fuels* **2008**, *22*, 2748–2755.
- (51) Huang, W.; Tang, S.; Zhao, H.; Tian, S. Activation of Commercial CaO for Biodiesel Production from Rapeseed Oil Using a Novel Deep Eutectic Solvent. *Ind. Eng. Chem. Res.* **2013**, *52*, 11943–11947.